RSC Advances

ROYAL SOCIETY OF CHEMISTRY

www.rsc.org/advances

Journal Name

RSCPublishing

ARTICLE

MnO_2 nano/micro hybrids for supercapacitors: "Nano's Envy, Micro's pride"

Cite this: DOI: 10.1039/x0xx00000x

S. Roshny, R. Ranjusha, M.S. Deepak, R. Sanoj, R. Jayakumar, S.V. Nair, A. Balakrishnan

Received 00th January 2012,
Accepted 00th January 2012

DOI: 10.1039/x0xx00000x

www.rsc.org/

The present study provides the first reports on a low temperature molten salt route which can generate unique architecture of MnO_2 nanospikes arrayed in peculiar fashion to form micron sized ball morphology. This morphology when employed as supercapacitor electrodes gives an advantage of surface relaxation during the charge/discharge process making it super stable. The study highlights the advantages of nanostructuring of microparticles which can answer the toxicity issues and their potential as a commercial product. This claim in the present study has been validated by cell toxicity study on human dermal fibroblasts, which established that a nano/micro hybrid structures can be relatively less toxic. Cytoskeleton rearrangements were also observed as the size of MnO_2 was reduced from micron to nanoscale. A mechanism of the structure formation and the influence of the salt in controlling the process parameters as well as the morphology are also proposed. These electrodes in coin cells exhibited specific mass capacitance value as high as 1100 F g^{-1} with a power density and energy density of 4.5 Whkg^{-1} and 14 kWkg^{-1}, respectively.

1. Introduction

Nanotechnology utilizes the unique properties of ultra-fine particles in the form of large surface area to create devices with high performance.[1-4] While much of the research is focused on improving the performance of the batteries, some of the most exciting research has happened with supercapacitors, because they demonstrate longer life, can be charged quickly and deliver higher power than a conventional battery. One option being explored is making supercapacitors with nanostructures. Different nanomaterials have been employed for electrode development in both energy storage and generation devices. [5] This includes different nanostructures of metal oxides, nanocarbons, chalcogenides and their composites.[6,7] Metal oxides have gained a lot of attention because of their superior chemical stability and high temperature performance as electrode materials in supercapacitors and batteries.[7] Among these metal oxides, MnO_2 has been widely researched because of its low cost and toxicity.[8] The advantages of these MnO_2 nanostructures in supercapacitors includes: lower internal resistance, good cycling stability and high capacitance. [8-10] Moreover, as the particle size scales down from micron to nano, the number particle per volume increases by an order of nine.[12] The resulting increase in surface area can be highly desirable for electrode applications since more active sites can be utilized during the redox reactions which can improve specific capacitance of the electrode overlay.[13-15].But from a commercial perspective, the advantages are compromised by problems associated with environmental and health issues. For instance, nanoparticles in free form, when released into the air or water during production can accumulate in the soil, water, or plant life. Secondly, in fixed form, where they are part of a manufactured product, they can cause pollution on disposal. [16] This in turn can have adverse impact on humans. So the hands are tied when it comes to fully utilising the potential nanotechnology could offer as the risks involved prove to be fatal

Manganese dioxide (MnO_2) as the cathode material for supercapacitors and batteries has been widely investigated because of its low-cost, abundance, non-toxicity and high theoretical specific capacitance of 1370 Fg^{-1}.[8] Although MnO_2 is a biocompatible material, our studies on cell up-take and toxicity have shown that when the particle size is reduced to <100 nm, MnO_2 showed higher cellular uptake than their micro-counter parts resulting in cell inflammation at topical level to humans.[17] Results of these studies have been discussed later in the text. This means that once these particles are within

the body they are highly mobile and in some instances can even cross the blood-brain barrier causing permanent damage.

Thus these nanoparticles can enter market only when it has been proven that there is no threat to health and the environment by regulatory bodies like Food and Drug Administration (FDA). The bill, entitled 'the FDA Safety and Innovation Act' which was passed in June 2012, states that "it is not enough to rely on the existing knowledge about a chemical or substance that is been cleared in its bulk state. A version of that material that is on the nanoscale may require additional testing and approvals even if it is already in the market". Apart from the toxicity issue, an industry viable process which is simple as well as environmentally friendly and one which involves easily available precursors at attainable working temperatures is the need of the hour.[18, 19]

MnO_2 can exist as polymorphs of α, β, γ and δ type. The polymorphs differ in their physio-chemical properties which can be ulitlized for various applications. [8-10] Amongst them, α -MnO_2 is widely used as the electrode material in energy storage devices. The structure of α -MnO_2 consists of double chains of edge sharing MnO_6 octahedra. These octahedra share corners to form 2 x 2 as well as 1 x 1 tunnels. The 2 x 2 tunnels favor the storage of electrolytic cations due to their larger size thereby increasing diffusion and capacitance. This property makes α -MnO_2 a desirable material for electrode fabrication in storage devices like supercapacitors/alkaline-batteries.[8]

The present article demonstrates the first report on the bulk synthesis of spike balled micro/nano hybrid structures of α-MnO_2 via low temperature molten salt route. These 3 D structures exhibited a mean diameter of ~1 μm arrayed with 1 D spikes of diameter 30-50 nm. The study highlights the advantages of utilizing these hybrid structures in supercapacitor applications as well as compares its cell up take and toxicity through MTT assay (3-(4,5-dimethylthiazol-2-yl)-2,5-diphenyltetrazolium bromide) tests with their nano-counter parts. Detailed electrochemical studies have elucidated the role that surface morphology and redox reactions play to enhance the cycling and capacitive performance of the electrodes. These electrodes showed a specific mass capacitance of 1100 Fg^{-1} with excellent cycling stability extending to 10,000 cycles. The study revealed an intrinsic correlation between the capacitance, internal resistance and the surface morphology. This correlation could be explained considering the relative contributions from the faradaic properties of MnO_2 in different electrolytes. Further, a working model supercapacitor in coin cell form is also shown exhibiting energy and power density 4.5 $Whkg^{-1}$ and 14 kW kg^{-1}, respectively.

2.Experimental

The chemicals used in the present study were of reagent grade obtained from Nice Chemicals, India. First, 5 g of lithium nitrate was taken in quartz crucibles and melted at 250 ºC. To this melt 1g of anhydrous $MnSO_4$ was added under constant stirring conditions. The prepared melt mixture was heated to 350°C for different holding time of 1, 2, 5 and 10h in air and furnace cooled. The resultant mass was dispersed in deionized water and centrifuged at 8000 rpm for 10 min. The sediment pellet was thoroughly washed using distilled water and dried in air at 70°C for 12 h.

2.1 Electrophoretic deposition and surface characterization

Morphology and phase analyses were performed using transmission electron microscopy-selective area energy dispersive X-ray (TEM, Model: JEOL, JEM-2100F), scanning electron microscopy (SEM-JEOL, Japan) and X-ray diffraction analyses (XRD, X'Pert PRO Analytical), respectively. The resultant nanostructures were electrophoretically deposited onto a titanium substrate. For this an electrochemical setup comprising of titanium foil (1cm x1cmx0.2 mm) was used as a substrate (cathode) and platinum wire as an anode. Isopropanol solution was used as the electrolytic solvent. To this electrolyte, 10 mg of the synthesized MnO_2 powder were dispersed uniformly by ultra-sonication. The deposition was carried out at 40 V for 15 min at room temperature, resulting in a thin uniform porous layer of MnO_2 nanostructures. The surface porosity was determined by quantitative image analysis (using GMDH software, Charlottesville, VA) from the SEM images. Surface profilometer (VeecoDektak 150) was used to measure the surface roughness and thickness of the deposited layer. Surface area measurements were carried out using a BET analyzer (Nova Quantachrome, USA) and Atomic Force Microscopy (AFM) (JEOL SPM 5200). Stability of the electrodes were further analysed using Inductively Coupled Plasma Atomic Emission Spectroscopy (ICP-AES).

2.2 Cytotoxicity studies and Cellular localization by fluorescent imaging

Cytotoxicity experiments were carried out on human dermal fibroblasts (HDF) by MTT assay. MTT [3-(4, 5-Dimethylthiazole-2-yl)-2, 5-diphenyl tetrazolium] assay for cytotoxic evaluation is a colorimetric test based on the selective ability of viable cells to reduce the tetrazolium component of MTT in to purple coloredformazan crystals. The cells were seeded on a 96 well plate with a density of 10, 000 cells/cm2. Four different concentrations of the samples (20, 40, 60 and 80 μg/mL) were prepared by dilution with the media. After reaching 90% confluency, the cells were washed with phosphate buffer saline (PBS) and different concentration of the samples (100 μL) was added and incubated. Cells in media alone devoid of nanogels acted as negative control and cells treated with Triton X-100 as positive control for a period of 24 h. 5mg of MTT (Sigma) was dissolved in 1 mL of PBS and filter sterilized.10 μL of the MTT solution was further diluted to 100 μL with 90 μL of serum–free phenol red free medium. The cells were incubated with 100 μL of the above solution for 4h to form formazan crystals by mitochondrial dehydrogenases. 100 μL of the solubilisation buffer (10% Triton X-100, 0.1N HCl and Isopropyl alcohol) was added in each well and incubated at room temperature for 1h to dissolve the formazan crystals. The optical density of the solution was measured at a wavelength of 570 nm using a Beckmann Coulter Elisa plate

reader (BioTek Power Wave XS). Triplicate samples were analyzed for each experiment.

For cell uptake studies, Rhodamine labelled micro and nano MnO_2 samples were used. Acid etched cover slips kept in 24 well plates were loaded with HDF cells with a seeding density of 20000 cells per cover slip and incubated for 24 h for the cells to attach well. After 24 h incubation, the media was removed and the wells were carefully washed with PBS buffer. Then the particle at a concentration of 60µg/mL was added along with the media in triplicate to the wells and incubated for a time period of 24h. After the particular incubation time, media with sample were removed and the cover slips were processed for fluorescent imaging. The processing involved washing the cover slips with PBS and fixing the cells in 3.7% Para Formaldehyde (PFA) followed by a final PBS wash. The cover slips were air dried and mounted on to glass slides with DPX as the mountant. The slides were then viewed under the microscope to study the internalization.

2.3 Electrochemical characterization

Cyclic voltammetry (CV) and constant current charge–discharge were performed to evaluate the capacitance. Electrochemical impedance spectroscopy (EIS) (electrochemical workstation: Newport Model) was performed under a biased potential of 0.2 V to measure the charge transfer resistance of the prepared electrode in the frequency range of 100000−0.1 Hz. For the above electrochemical studies, a three-electrode setup consisting of electrophoretically deposited MnO_2 powder, platinum and calomel electrodes were used as working, counter and reference electrodes respectively. Different electrolytes comprising of KOH, NaOH and KOH in 1 M concentrations were used. From the best system determined, CV was performed for different scan rates of 100,50,20,10 and 1 mVs^{-1}. The specific capacitance was measured. The cycling stability was also determined using CV for 10000 cycles. ICP-AES studies were done to determine the dissolution of the material in the electrolyte.

3. Results and discussions

3.1 Phase and morphological analysis

Fig.1(a-d) show the TEM images displaying the evolution of MnO_2morphology synthesised under different processing times of 1, 2, 5 and 10 h. It was observed that as the processing time increased from 1 to 10 h, the morphology showed prominent spikes arrayed randomly to form microspheres. These microspheres showed diameter varying from 1-2 µm. The spike showed thickness ranging from 30-70 nm.

Fig. 2 shows the XRD pattern of the processed powder at various times. The diffraction peaks corresponded to pure tetragonal phases of α- MnO_2 (JCPDS 44-0141). This time dependent morphological evolution is schematically represented in Fig. 3. During the initial formation stage, the reactant gets diffused into the salt and dissolves in it. This stage

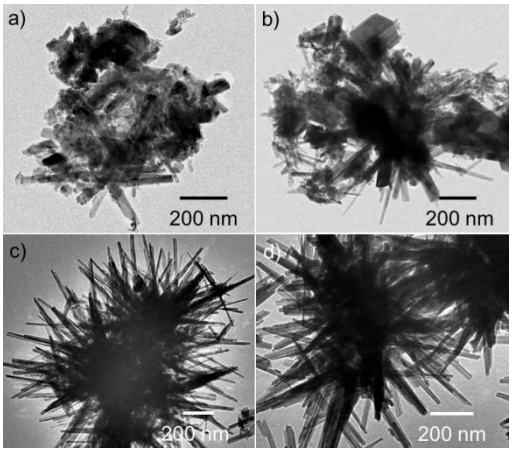

Fig.1. Evolution of MnO_2 morphology as a function of time a) 1h, b) 2h, c) 5h and d) 10h

is followed by the formation of nuclei which can be expressed by the reaction (1) shown below:

$$MnSO_4 \rightarrow MnO_2 + SO_2 \quad (1)$$

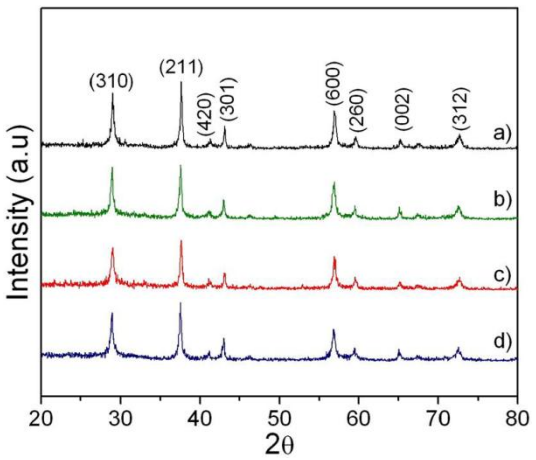

Fig. 2. XRD patterns of MnO_2 processed at different times a) 1h, b) 2h, c) 5h and d) 10h

The MnO_2 nuclei formed can undergo Ostwald ripening (crystal growth stage) and aggregate into nanosized spheroidal particles. The spheroids thus formed may act as crystal growth sites, which can absorb newly formed nuclei onto its surfaces. The degree of adsorption is determined by the surface energies of the different facets of the base crystal. The nuclei gets attached itself to the high surface energy facet as a part of surface energy minimisation and continues to grow along the incited direction. The spike formation and growth seem to stabilize at the end 5 h. This structure was retained for longer time periods of 10 h as seen from the TEM images (see Fig. 1(d)). Thus the further characterization was done on 5 h samples. Hereby these samples are designated as M-5.

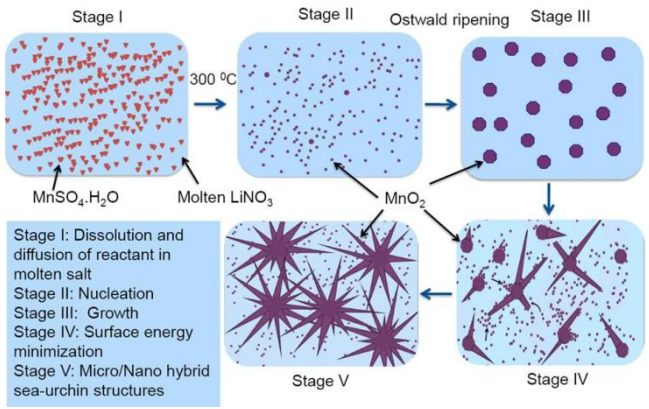

Fig 3: Schematic representation of the time dependent morphological evolution of the nano/micro structure.

3.2 Cytotoxicity studies

The M-5 samples were compared with ~50 nm MnO_2 powders (for TEM please see ESI-I) and studied for their cell toxicity and cell uptake. The BET surface area (see ESI-II) for M-5 and the nanopowders was measured to be 18 and 38 m^2/g, respectively. MTT assay confirmed the biocompatibility of M-5 (Fig. 4).

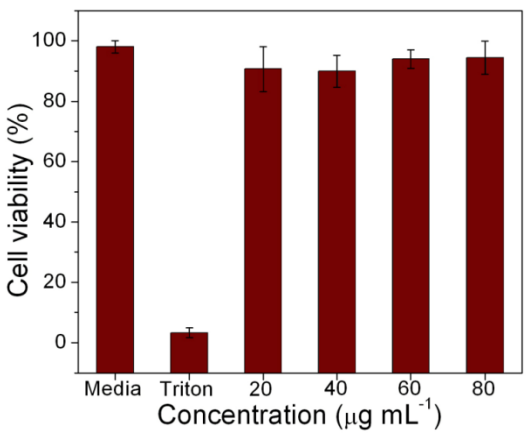

Fig 4: MTT assay of nano/ micro hybrid MnO_2

Even as these tests confirm the biocompability of MnO_2, it was observed that cell uptake was higher in case of nano-MnO_2. From Fig. 5, it was evident that the nano-MnO_2 exhibited higher cellular uptake, modulating the cytoskeletal arrangements of HDF cells as depicted with actin dye (purple spots).

As explained earlier, such an uptake can be detrimental considering the fact that it can penetrate the blood brain barrier. Further observations showed distorted cell nucleus with expanded cell morphology confirming enhanced cellular uptake of the nano MnO_2 in comparison to M-5. Such a cell inflammatory response was also an indication of its toxicity for humans at the topical level.

However, M-5 samples showed no uptake by the HDF cells. This means that lack of safety protocols while handling the energy storage devices during processing and disposal can lead to the penetration of these nanopowders into the blood stream. These results showed that M-5 did not pose any health threats on exposure.

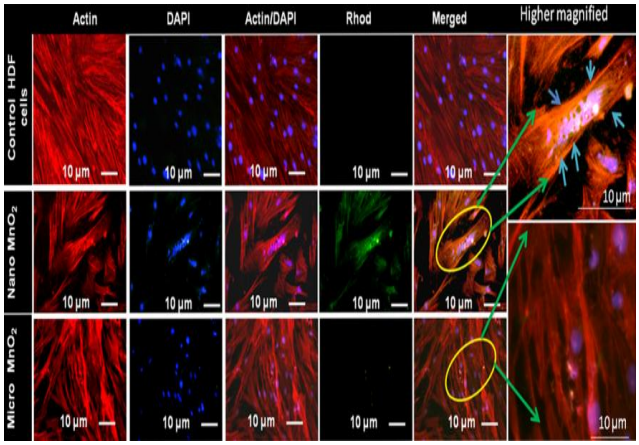

Fig 5: HDF cell uptake study of nano MnO_2 and nano/micro hybrid MnO_2

3.3 Electrochemical studies

For electrochemical studies, M-5 samples were deposited as thin films onto titanium plates. The surface morphology of these coatings (Fig. 6(a)) showed a roughened and porous layer. The mean surface roughness (R_a) measured from AFM was found to be 200 ± 45 nm (see ESI-III)

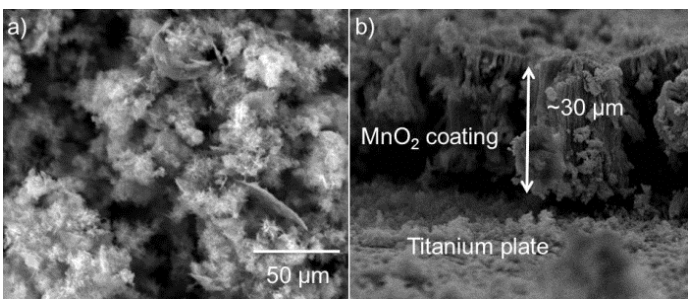

Fig 6: SEM image of a) Ti plate coated with M-5 samples and b) Cross sectional image of the coating.

The SEM cross-sectional image (Fig. 6(b)) showed this deposited layer having a thickness of ~30 μm

3.3.1. Role of different electrolytes

The electrochemical performance of these thin film electrodes in different electrolytes of the same concentration (1 M) were studied using CV analysis at a scan rate 10 mVs^{-1}. The performance of the electrode in LiOH, NaOH and KOH is shown in Fig. 7 (a-c). The basic redox reaction for MnO_2 in the above electrolytes can be expressed using the following reaction (2):

$$MnO_2 + yC^+ + e^- \leftrightarrow yMnOOK + (1-y)\,MnO_2 + e^- \quad (2)$$

Here *C* and y represents the electrolyte cation and total number of active sites present on the surface of the MnO_2 structure, respectively.

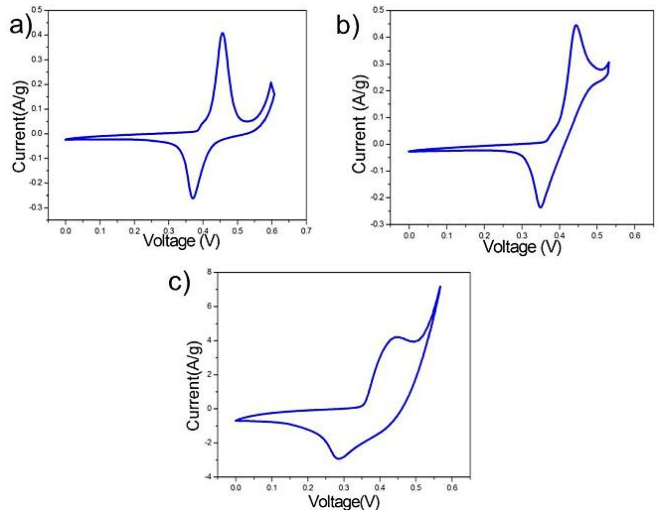

Fig 7: CV analysis of the electrode in 1M a)LiOH b)NaOH and c)KOH electrolyte systems

The best performing electrolyte was found to be 1M KOH, in which the CV curves showed higher current when compared to NaOH and LiOH. The reason for this could be mainly attributed to the low hydrated radius of K^+ ions (0.25 nm) as compared to Na^+ (0.36 nm) and Li^+ (0. 42 nm).[20] This becomes relevant as the tunnel cavity of α-MnO_2 has an inner diameter of 0.38 nm which can facilitate the intercalation and de-intercalation of hydrated K^+.[20-22] Moreover, the peculiar architecture of MnO_2 when employed as thin films can also enhance the electrode-electrolyte interaction which can play a pivotal role in improving the capacitance. Thus, further studies were conducted with 1M KOH.

3.3.2. Influence of different scan rates

CV curves of these electrodes were recorded at different scan rates and are shown in Fig. 8 (a). The mass specific capacitance from the CV curves was calculated using the following equation.[23,24]

$$C = \frac{1}{M \times \Delta V \times s} \int IdV \qquad (3)$$

where C is the mass specific capacitance (F g^{-1}), M is the mass of the active electrode, ΔV is the voltage window, s is the scan rate and I represents the current. The mass specific capacitances were calculated as 1100 Fg^{-1}, 771 Fg^{-1}, 514 Fg^{-1}, and 332 Fg^{-1} at scan rates of 5 mVs^{-1}, 20 mVs^{-1}, 50 mVs^{-1} and 100 mVs^{-1} respectively (Fig 8(b)). High capacitance values at lower scan rates could be attributed to the ample time K^+ gets to interact (intercalate and de-intercalate) with the maximum active sites. The decrease in specific capacitance at faster scan rates can be attributed to the fact that the ions from the electrolyte can reach only up to the electrode surface with limited entry into the deeper pores of the electrode overlay which is reflected as lower capacitance values.[25]. These electrodes were subjected to cycling studies at 100 mVs^{-1} scan rate (Fig. 8 (c)). The M-5 electrodes showed no fading even after the end of 10,000 cycles. This was further confirmed by ICP-AES analysis where no electrode dissolution in the electrolyte occurred at the end of 1st and 10,000th cycle.

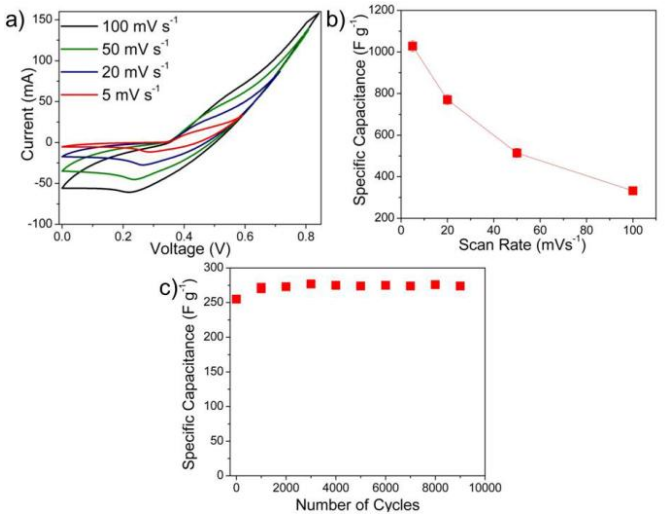

Fig 8: a) CV curves at different scan rates, b) plot of scan rate vs capacitance and c) cycling studies at 100 mVs^{-1}

Capacitance fading is generally attributed to the dissolution of the oxide film into the electrolyte. Any structural variations within an electrode overlay can play a significant role in determining the final stability. During the cyclic volumetric expansion–contraction, these electrodes tend to be stretched and relaxed, leading to tensile and compressive stresses on the entire overlay. Since these spiked micro/nano-hybrid structures are deposited in a 3-D stacked plane, the electrode overlay can distribute these microscopic stresses isotropically along the matrix. Further, the inter-locking of these spikes could also increase shear strength of the electrode structure, which in turn may help to prevent crack formation thereby preventing any peeling under cycling.[8, 25]

Further, an increase in capacitance was observed during the initial cycles prior to the stabilization. It has been shown that the porous microstructure is electrochemically favorable since it can provide substantially larger spatial clearance for electrode expansion and contraction during cycling. Upon prolonged cycling, expansion and contraction of the electrode overlay open new active sites within the porous structure which participates in the charge-transfer mechanism and increases the capacitance values. A similar phenomenon has been reported earlier in a literature where MnO_2 nanostructures in the form of thin film nanoporous electrodes in combination with 1 M KOH electrolyte have been used wherein the mass specific capacitance increased by ~45%.[8]

3.3.3. Coin cell performance

A coin cell was fabricated using M-5 powders as electrodes (Fig. 9(a)). Fig. 9(b) displays the constant current discharge performance of M-5 electrodes at different discharging

currents. From these discharge curves, the capacitance, energy density and power density was derived using the following equations.

$$C = \frac{I \times \Delta t}{\Delta V} \quad (4)$$

$$E = \frac{1}{2} C V^2 \quad (5)$$

$$P = \frac{V^2}{4R} \quad (6)$$

Where C is the specific capacitance, I is the discharge current, ΔV is the potential window and Δt is the total discharge time, V is the maximum voltage, E is the energy and P is the power that can be drawn from the device, and R is the equivalent series resistance.[7,8]

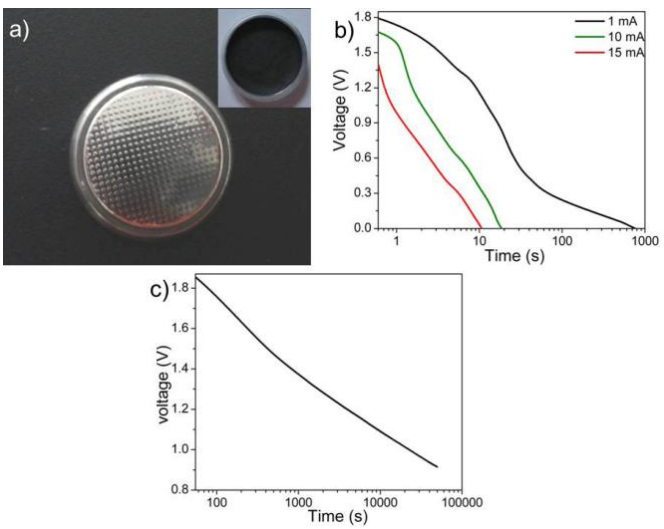

Fig 9: a) Coin cell with the cathode coating in the inset, b) constant current discharge performance at different discharging currents and c) self-discharge behaviour of M-5 coin cells

The slight deviation of the linear characteristics for each discharge curve was observed. This deviation from the linear trend could be attributed to either of the following factors i.e. a) variation in the direct equivalent series resistance, b) the re-arrangement of charges within the pores of the material structure during the discharge and c) the redox behavior of the material.[26, 27] The capacitance values were measured to be 450, 12 and 11 mF at discharge currents of 1mA, 10 mA and 15 mA respectively. The reduction in capacitance values with increase in applied current is well known phenomenon for transition metal oxide systems.[29,30] The fading of capacitance at higher currents can be attributed to an assortment of multiple factors like voltage (IR) drop, distributed pore resistance on the electrode overlay and severe redox reactions on the metal oxide electrode surface.[28]However, isolating the role of individual factor affecting the electrode's performance is difficult. Fig. 9 (c) shows the self-discharge behavior for period of ~14 h where the total-discharge was found to be ~50% indicating low self-discharge property. The maximum energy density and peak power density values for these coin cells were found to be 4.5 Whkg^{-1} and 14 kW kg^{-1}, respectively.

The impedance measurements of the MnO_2 nano/micro hybrid system in KOH electrolyte were performed in the frequency range of 0.1 to 10^5 Hz. The Nyquist plot of these hybrid samples are presented in Fig. 10 and the corresponding equivalent circuit model is shown as the inset of Fig. 10. The equivalent circuit for this Nqvuist plot was obtained by using the circuit fitting tool in the FRA software representing a third order RC network system. The impedance behavior of the sample was analysed in three frequency regions such as high, medium and low-frequency to evaluate the different mechanisms occurring in different frequency domains. The first point of intersection with the real axis gives the electrolyte/solution resistance (R_s) where MnO_2 behaves like a pristine resistor. The two partial semicircles at high and medium frequency regions can be attributed to the different charge transfer mechanisms in the nano/micro hybrid system as a result of redox reactions. The appearance of high frequency semicircle (region-I) is mainly attributed to the charge propagation phenomenon occurring at the interface of MnO_2 nano/micro hybrid and KOH electrolyte and can be modelled as interfacial capacitance at the solid-electrolyte layer C_{EL} in parallel with the electrolyte resistance R_{EL}. This R_{EL} is the resistance resulting from the discontinuity in the charge propagation phenomenon occurring at the MnO_2/KOH interface, which arises from the difference in electronic conductivity of MnO_2 and ionic conductivity of the KOH electrolyte. The second semicircle (region-II) at the medium frequency regions correspond to the charge-transfer resistance (R_{CT}) due to redox processes in the system which involves the exchange of K^+ ions and this charge transfer is associated with the surface phenomena of the nano/micro hybrid system. This characteristic feature of the hybrid system can be modeled as thin film impedance due to the redox processes involving electron hopping mechanism in the MnO_2 hybrid system and K^+ ions diffusion. This will consist of a film capacitor, C_F, in parallel with the R_{CT}.[31, 32] At a lower frequency region of the nyquist plot, Warburg impedance gets displayed as a partial semicircle (region-III), and is described as diffusive resistance (W) of the K^+ ion within the hybrid electrode pores. Generally a straight vertical line along the imaginary axis Z^{II} is observed for an ideally polarized system where as in a practical supercapacitor, a finite slope appears in this line which represents the diffusive resistance of electrolyte in electrode pores and ion diffusion in MnO_2 as the diffusion of K^+ is not same in the liquid electrolyte and solid electrode materials. The presence of Warburg indicates the dense nature of these spiked ball structure.[33] The storage mechanism in this region is predominated by double layer mechanism C_{dl} which can be modelled parallel to Warburg resistance (W).

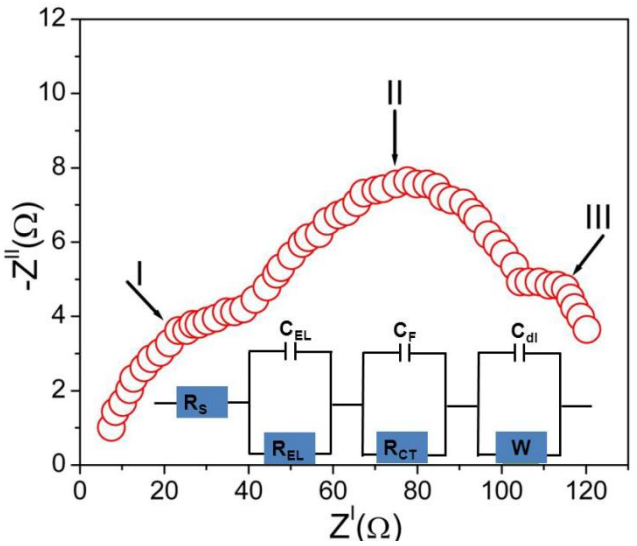

Fig 10: Nyquist plot of M-5 coin cell (Inset- Equivalent circuit). R_s, R_{EL} and R_{CT} represents the solution resistance, the electrolyte resistance and the charge transfer resistance respectively, W is the Warburg resistance, C_{EL} is the interfacial capacitance at the solid-electrolyte layer, C_F is the faradaic capacitance and C_{dl} represents capacitance due to the electric double layer formation.

4. Conclusions

The present study investigates the storage performance of MnO_2nano/micro hybrids for supercapacitors. The MnO_2nano/micro clusters were synthesized using a low temperature molten salt method, wherein several nanospikes assembled to form these clusters. MTT assay tests showed low cell uptake in human dermal fibroblasts as compare to their nano-counterparts. These hyrbid clusters were employed as an electrode in a fully functional coin cell exhibiting an energy density and power density of 4.5 $Whkg^{-1}$ and 14 $kW\ kg^{-1}$, respectively, with a low self-discharge behavioural trend. These electrodes showed super stability even at the end of 10,000 cycles. EIS studies demonstrated that these systems can exhibit an equivalent circuit corresponding to a third order transient response. The performance of these micro/nano hybrid MnO_2 systems is promising considering their low cost and facile fabrication process.

Acknowledgements

Council of Scientific and Industrial Research (CSIR), Government of India is gratefully acknowledged for its financial support under project no. 22(0565)/12/EMR-II. MNRE is also acknowledged for providing with the infrastructural support. DST-Government of India is also acknowledged for supporting Dr Avinash Balakrishnan under the Fast Track Scientist-Scheme.

Notes and references

Amrita Center for Nanosciences and Molecular Medicine, Ponekkara, Kochi, India. Fax: +91-484-2802020; Tel: +91-484-2802020;E-mail:avinash.balakrishnan@gmail.com.

1. B.E.Conway, *Electrochemical Supercapacitor: Scientific Fundamentals and Technological Applications*, Kluwer Academic/Plenum Publishers, New York,1999.
2. P. Simon and Y. Gogotsi, *Nat. Mater.*, 2008, **7**, 845.
3. M Jayalakshmi and K Balasubramanian, *Int. J. Electrochem. Sci.*,2008,**3**, 1196 – 1217
4. A. Burke, *J.Power Sources* , 2000, **91**, 37–50
5. M. Wohlfahrt-Mehrens, J. Schenk, P.M. Wilde, E. Abdelmula, P. Axmann and J. Garche, *J.Power Sources*, 2002, **105**, 182–188
6. B.E.Conway, V.Birss and J.Wojtowicz, *J. Power Sources*, ,1997,**66**,1-14.
7. G.Wang, L.Zhang and Jiujun Zhang,*Chem.Soc.Rev*, 2012, **41**, 797-828.
8. R Ranjusha., A.S.K.Nair, S.Ramakrishna, P.Anjali,K. Sujith,K. R. V. Subramanian,N.Sivakumar,T. N. Kim, S. V. Nair and A. Balakrishnan, *J. Mater. Chem.*, 2012, **22**, 20465
9. X.Lang, A.Hirata,T.Fujita and M.Chen, *Nat. Nanotechnol*, 2011,**6**,232-236
10. R.N. Reddy and R.G Reddy. *J. Power Sources*, 2003,**124**,330-335
11. R.N. Reddy and R.G.Reddy, *J.Power Sources*, 2004, **132**, 315-320.
12. D.L. Schodek, P.Ferreira and M.F. Ashby,*Nanomaterials, Nanotechnologies and Design: An Introduction for Engineers and Architects*, Butterworth-Heinemann Ltd,U.K, 2009, 187.
13. M.W .Xu, L.B.Kong,W.J. Zhou, and H.L Li, *J.Phys. Chem. C*, 2007, **111**,19141-19147.
14. S.L Brock,N.G Duan, Z.R Tian,O. Giraldo,H Zhou and S. L Suib, *Chem.Mater*, 1998,**10**, 2619-2628
15. C. Burda, X. B. Chen, R. Narayanan, and M. A. El-Sayed, *Chem. Rev*, 2005, **4,** 1025–1102.
16. C.Buzea, I.I. Pacheco and K.Robbie, *Biointerphases*,2007, **2**, MR17-MR71.
17. S. Rejnold, R.Ranjusha, A.Balakrishnan, N.Mohammed and J.Rangasamy, *RSC Adv.*, 2013, Accepted
18. N.Sui, Y.Duan, X.Jiao, and D.Chen, *J. Phys. Chem. C*, 2009, **113**, 8560–8565.
19. B. Li,G. Rong, Y.Xie, L.Huang, and C. Feng, *Inorg.Chem*,2006, **45**,6404–6410.
20. Y. U. Jeong and A. Manthiram, *J. Electrochem. Soc.*, 2002, **149,**A1419.
21. J. Jiang and A. Kucernak, *Electrochim. Acta*, 2002, **47**, 2381.
22. G. G. Kumar and S. Sampath, *Solid State Ionics*, 2003, **160,** 289.
23. R. Ranjusha, S.Ramakrishna,A. S.K. Nair, P. Anjali, S. Vineeth, T. S. Sonia, N. Sivakumar, K. R. V. Subramanian, S. V. Nair and A. Balakrishnan, *RSC Adv.*, 2013,**3**, 17492-17499.
24. R. Ranjusha, K.M. Sajesh, S. Roshny, V. Lakshmi, P. Anjali, T.S. Sonia, A. Sreekumaran Nair,K.R.V. Subramanian, Shantikumar V. Nair, K.P. Chennazhi, A. Balakrishnan, *Micropor Mesopor Mat.*, 2014, **186**, 30-36.

25. S. Cheng, D. Yan, J. T. Chen, R. F. Zhuo, J. J. Feng, H. J. Li,H. T. Feng and P. X. Yan, *J. Phys. Chem. C*, 2009, **113**, 13630.
26. S. Chen, J. Zhu, X. Wu, Q. Han and X. Wang, *ACS Nano*, 2010, **4**,2822.
27. J. Chen, N. Xia, T. Zhou, S. Tan, F. Jiang and D. Yuan, *Int. J.Electrochem. Sci.*, 2009, **4**, 1063.
28. S. K. Meher, P. Justin and G. R. Rao, Electrochim. Acta, 2010, **55**,8388.
29. C. Yuan, X. Zhang, L. Su, B. Gao and L. Shen, *J. Mater. Chem.*,2009, **19**, 5772.
30. J. W. Lang, L. B. Kong, W. J. Wu, Y. C. Luo and L. Kang, *Chem.Commun.*, 2008,**35,** 4213.
31. P. Kurzweil, *The 14th International Seminar On Double Layer Capacitors*,Deerfield Beach, FL., U.S.A.,, 2004
32. A. J. Bard, L. R. Faulkner, *Electrochemical Methods*, JohnWiley& Sons, New York 1980, Chapter 9.
33. S. K. Meher, P. Justin and G. R. Rao, *Nanoscale*, 2011, **3**, 683-692.

Electronic Supplementary Information (ESI) available: [SEM and TEM of MnO_2 nanoparticles, BET of M-5 sample and AFM analysis of M-5 coating]. See DOI: 10.1039/b000000x/

